JOURNAL OF GEOPHYSICAL RESEARCH, VOL. 111, D16113, doi:10.1029/2005JD006276, 2006

Evaluation of model-derived and remotely sensed precipitation products for continental South America

L. Gustavo Goncalves de Goncalves,[1,2] W. James Shuttleworth,[1] Bart Nijssen,[1] Eleanor J. Burke,[3] Jose A. Marengo,[4] Sin Chan Chou,[4] Paul Houser,[5] and David L. Toll[6]

Received 26 May 2005; revised 9 January 2006; accepted 8 May 2006; published 30 August 2006.

[1] This paper investigates the reliability of some of the more important remotely sensed daily precipitation products available for South America as a precursor to the possible implementation of a South America Land Data Assimilation System. Precipitation data fields calculated as 6 hour predictions by the CPTEC Eta model and three different satellite-derived estimates of precipitation (Precipitation Estimation from Remotely Sensed Information using Artificial Neural Networks (PERSIANN), National Environmental Satellite, Data and Information Service (NESDIS), and Tropical Rainfall Measuring Mission (TRMM)) are compared with the available observations of daily total rainfall across South America. To make this comparison, the threat score, fractional-covered area, and relative volumetric bias of the model-calculated and remotely sensed estimates are computed for the year 2000. The results show that the Eta model-calculated data and the NESDIS product capture the area without precipitation within the domain reasonably well, while the TRMM and PERSIANN products tend to underestimate the area without precipitation and to heavily overestimate the area with a small amount of precipitation. In terms of precipitation amount the NESDIS product significantly overestimates and the TRMM product significantly underestimates precipitation, while the Eta model-calculated data and PERSIANN product broadly match the domain average observations. However, both tend to bias the zonal location of precipitation more heavily toward the equator than the observations. In general, the Eta model-calculated data outperform the several remotely sensed data products currently available and evaluated in the present study.

Citation: de Goncalves, L. G. G., W. J. Shuttleworth, B. Nijssen, E. J. Burke, J. A. Marengo, S. C. Chou, P. Houser, and D. L. Toll (2006), Evaluation of model-derived and remotely sensed precipitation products for continental South America, *J. Geophys. Res.*, *111*, D16113, doi:10.1029/2005JD006276.

1. Introduction

[2] Weather and climate predictions are known to be sensitive to surface storage of water and energy, both at regional and global scales [e.g., *Koster and Suarez*, 1999; *Beljaars et al.*, 1993; *Betts et al.*, 1996; *Fast and McCorkle*, 1991; *Fennessey and Shukla*, 1999]. In the last three decades, land surface models (LSMs) have been used extensively in coupled land surface-atmospheric models to provide a description of the feedback from the underlying soil and vegetation to the atmosphere during model integration [e.g., *Sellers et al.*, 1986; *Xue and Shukla*, 1993]. Recently, so-called land data assimilation schemes (LDAS) [*Mitchell et al.*, 2000, 2004; *Rodell et al.*, 2004; *Koster et al.*, 2004] have been successfully employed to provide improved initial surface fields of soil moisture for use in predictive meteorological models (in near real time) and to address land surface management issues. LDAS comprise two-dimensional arrays of LSMs arranged to match the grid squares used in the predictive model, which are forced by model-derived near-surface fields supplemented, to the maximum extent possible, with surface observations of meteorological variables.

[3] An important challenge when using LDAS or when assessing the performance of coupled (or uncoupled) land-atmosphere parameterizations is the scarcity of comprehensive land surface data at the spatial and temporal resolutions at which the models operate [*Maurer et al.*, 2002]. Providing adequate observations of precipitation is particularly problematic because precipitation is so spatially variable,

[1]Department of Hydrology and Water Resources, University of Arizona, Tucson, Arizona, USA.
[2]Now at Hydrological Sciences Branch, Code 614.3, NASA Goddard Space Flight Center, Greenbelt, Maryland, USA.
[3]Hadley Centre for Climate Prediction and Research, Met Office, Exeter, UK.
[4]Centro de Previsão do Tempo e Estudos Climáticos, Instituto Nacional de Pesquisas Espaciais, Cachoeira Paulista, Sao Paulo, Brazil.
[5]Center for Research on Environment and Water, George Mason University, Calverton, Maryland, USA.
[6]Hydrological Sciences Branch, Code 614.3, NASA Goddard Space Flight Center, Greenbelt, Maryland, USA.

0148-0227/06/2005JD006276$09.00

and often only point sample data from well-separated rain gauges are available. Some regions of the globe (e.g., North America, Europe, Japan, and parts of the former Soviet Union and China) have a reasonably dense coverage of observations. However, in the context of the present paper, it is significant that South America has very sparse temporal and spatial data coverage, and that this coverage is biased toward populated centers near the edge of the continent and along the main river course in the Amazon region. Consequently, simple interpolation of daily total precipitation is fraught with difficulty. Remotely sensed estimates of precipitation inferred, for example, from infrared cloud top temperatures may provide a means of filling the gaps between surface observations in remote regions. Unfortunately, the calibration and validation of such remotely sensed estimates is also difficult because ground-based observations are so sparse. Nonetheless, in the context of LDAS and despite these validation difficulties, remotely sensed estimates (perhaps merged with surface observations) remain the best hope for providing a spatially comprehensive set of precipitation observations in regions like South America, where surface observations are limited [*Peterson et al.*, 1998; *New et al.*, 2001].

[4] This paper evaluates three remotely sensed daily precipitation products currently available for South America. This is done as a precursor to the possible implementation of a South America LDAS for the Eta regional model [*Mesinger et al.*, 1988; *Black*, 1994] coupled with the Simplified Simple Biosphere (SSiB) LSM [*Xue et al.*, 1991], which is used for weather forecasting at CPTEC (Centro de Previsão de Tempo e Estudos Climáticos), the Brazilian Center for Weather Forecasts and Climate Studies. Consequently, the primary concern is how well the remotely sensed precipitation products reflect the daily precipitation inputs to the land surface. Because the goal of any LDAS would be to improve the initial energy and moisture state of the land surface model for a given moment in time, the precipitation products should reflect as accurately as possible the spatially distributed precipitation amount on any given day. Note that this is a stricter and more challenging requirement than matching the observed precipitation in some average or climatological sense. In addition, to be useful in an LDAS context, the precipitation products should better match the actual precipitation than the model derived product.

[5] In this study, precipitation data fields calculated as 24 hour accumulated predictions by the CPTEC Eta model and several different satellite-derived estimates of precipitation are compared with the available observations of daily total rainfall across South America, and the threat score, fractional covered area, relative volumetric bias, root-mean-square error and spatial cross correlation coefficients of the model-calculated and remotely sensed estimates are computed for the year 2000. In turn, these estimates are compared with gauge observations, which, although not without problem, remain the standard measure of surface precipitation input.

[6] The paper is divided into seven sections. The general climatology of South America is described briefly first, followed by a description of the Eta model, the remotely sensed data products, and the surface observations (section 3). Section 4 presents the analysis methods and performance measures. Results, discussion, and conclusions are presented in sections 5, 6, and 7, respectively.

2. Climatology of South American Precipitation

[7] There are substantial variations in the climate of continental South America associated with latitude, topography, and proximity to oceanic influence. In the northern part of the continent, much of the within-continent precipitation is convective in origin, either in the form of organized large-scale precipitation or originating from mesoscale tropical squall lines which produce rainfall near the coast and then propagate inland. Seasonal migration of the Intertropical Convergence Zone (ITCZ) modulates the large-scale pattern of rainfall variability in tropical South America. Rainfall east of the Andes is determined by the interaction between the trade winds blowing from west to east on both sides of the equator in this region. Northeast Brazil has a wet season which is restricted to a few months (February–May) and otherwise has a semiarid climate. The Amazon region experiences its rainy season during the months of November, December, and January (NDJ) in southern Amazonia and February, March, and April (FMA) in central Amazonia and the mouth of the Amazon River.

[8] The central and southeastern regions of South America are influenced by midlatitude and extratropical transient weather systems but have a well-defined convective wet season, especially southern Brazil, Paraguay, and northern Argentina, where mesoscale convective systems (MCSs) occur. These MCSs can be fed by moisture from the Amazon basin transported east of the Andes by a low-level jet (LLJ), especially during NDJ and FMA periods [*Seluchi and Marengo*, 2000; *Marengo et al.*, 2002, 2004; C. Vera et al., A unified view of the American monsoon systems, submitted to *Journal of Climate*, 2005]. This LLJ brings moisture from Amazonia during summer and is in part responsible for rainfall in northern Argentina and in the La Plata basin. It also brings moisture from the subtropical Atlantic during winter. This suggests that the LLJ is an all year round system, but the Amazon influence in rainfall in southeastern South America is restricted to Summer [*Marengo et al.*, 2004].

[9] Transient systems, such as cold fronts, regulate the precipitation regime over the southern portion of the continent. Rainfall in southeastern South America is also modulated by the South Atlantic Convergence Zone (SACZ) and is more intense during NDJ months [*Liebmann et al.*, 1999; *Nogués-Paegle and Mo*, 1997]. The intensity of the SACZ is influenced by the availability of regional moisture from the Amazon and its position is modulated by intense convective activity in the western Pacific, in the form of a Rossby wave that emerges from this section of the Pacific and propagates all the way to southeastern South America. There appears to be a dipole structure between the SACZ, in which a weak SACZ is consistent with a well developed LLJ, and vice versa. Cold fronts are also responsible for cooling in southern and southeastern Brazil during winter [*Marengo et al.*, 1997; *Garreaud*, 2000].

[10] Precipitation along the Andes Mountains is modulated by the topography. In the northern Andes, precipitation is associated with low-level wind convergence, while in the central and southern Andes it is primarily orographic in

nature. Regions such as the inter-Andean Valley in Colombia are among the wettest in the continent because of strong convective activity and mountain uplift [*Legates and Wilmott*, 1990; *Figueroa and Nobre*, 1990; *Marengo and Nobre*, 2001; *Velazco and Fritsch*, 1987; *Rao and Hada*, 1990; *Marengo*, 1995].

3. Model-Derived, Remotely Sensed, and Surface Observations of Precipitation

3.1. Eta Weather Forecast Model

[11] In this study, the model-calculated precipitation data fields used for comparison with remotely sensed products are the 36 hour predictions given by the CPTEC Eta model for the year 2000. Two model runs are performed daily, one initiated with initial conditions at 00Z and the other at 12Z with output every 6 hours. For the present study, forecasts initiated at 00Z were used. The daily totals are the accumulated precipitation for the 24h prior the 36h forecast (i.e., from 12Z of the day before to 12Z of the current day). Thus total daily precipitation on 2 January, for example, would be the accumulated precipitation from 1 January at 12Z through 2 January at 12Z. None of the surface observations of precipitation used here for validation are assimilated into the model prior to the 36 hour predictions.

[12] The Eta model, as implemented at CPTEC, is set up to describe a domain that covers most of South America with a grid resolution of 40 km in the horizontal and 38 vertical layers, with the model top corresponding to 50 hPa. The prognostic variables are surface pressure and the horizontal wind components, temperature, specific humidity, turbulent kinetic energy, and cloud water calculated over a semistaggered Arakawa E grid. Step-mountain (or Eta) vertical coordinates (as defined by *Mesinger* [1984]) are used in the model, with the resolution of vertical layers higher nearer the surface (the first layer is ~20 m deep) and in layers near the tropopause. In the adjustment stage, the forward-backward scheme modified by *Janjic* [1979] is used. The horizontal advection scheme was developed by *Janjic* [1984] specifically for the E grid and controls the cascade of energy toward smaller scales. It is used in conjunction with a modified Euler backward time-differencing scheme. A split explicit approach [*Gadd*, 1978] is used during model integration.

[13] The initial conditions for the Eta model are taken from NCEP (National Centers for Environmental Prediction) analyses and the evolving conditions at the lateral boundaries are updated every 6 hours using CPTEC global model forecasts [*Bonatti*, 1996; *Cavalcanti et al.*, 2002]. Both conditions are provided to the model in 28 vertical layers and in the form of spectral coefficients with T62 triangular truncation, equivalent to 1.825° resolution in the meridional and zonal directions. Sea surface temperature is prescribed to be the observed weekly average value [*Reynolds and Smith*, 1994], and the initial surface albedo is taken from a seasonal climatology [*Dorman and Sellers*, 1989]. Soil moisture and temperature are also taken from seasonal climatology [*Willmott et al.*, 1985] and linearly interpolated to the first day of simulation with no adjustments.

[14] Both grid-scale [*Zhao and Carr*, 1997] and convective precipitation [*Betts and Miller*, 1986; *Janjic*, 1994] are calculated. The turbulent exchange between model layers in the free atmosphere is based on the Mellor-Yamada level 2.5 scheme, while the exchange between the Earth's surface and the lowest model layer uses the Mellor-Yamada level 2 scheme [*Janjic*, 1994, 1996a, 1996b]. The radiation package was developed at the Geophysical Fluid Dynamics Laboratory: short-wave radiation is computed using the scheme of *Lacis and Hansen* [1974], while the long-wave radiation scheme is that of *Fels and Schwarzkopf* [1975].

3.2. PERSIANN Precipitation Data Product

[15] An automated system for Precipitation Estimation from Remotely Sensed Information using Artificial Neural Networks (PERSIANN) was developed by *Hsu et al.* [1997]. The primary remotely sensed data used to estimate rainfall are infrared images from geosynchronous satellites (GOES-IR) available every half-hour and sampled at a resolution of 0.25° × 0.25° [*Hsu et al.*, 1997]. The algorithm is based on an artificial neural network that can be adapted easily to incorporate any relevant additional information available. An adaptive training feature can be used to facilitate rapid updating of the artificial neural network parameters whenever independent estimates of rainfall are available. However, so far, no attempt has been made to incorporate data from South America into the training process. Consequently, the PERSIANN products evaluated in this study use extrapolated training calibrations made elsewhere (i.e., Japan islands and peninsula of Florida, USA) in the retrieval algorithm [*Hsu et al.*, 1997]. For this study, PERSIANN estimates of precipitation were only available for the last 10 months of 2000.

3.3. NESDIS Precipitation Product

[16] The NOAA National Environmental Satellite, Data and Information Service (NESDIS) experimental product [*Vicente et al.*, 1998] provides real-time rainfall estimates over South America based on cloud top temperature measurements in the 10.7 μm channel of the GOES 8 satellite. Estimates are not available when GOES 8 is in rapid scan mode because it only observes the Northern Hemisphere. Precipitation rates are calculated from a power law equation based on a comparison of satellite observations with collocated, instantaneous radar rainfall Estimates. These estimates were obtained from the U.S. operational network of 5 cm and 10 cm radar in the central Great Plains and areas adjacent to the Gulf of Mexico at a spatial resolution of 4 km. The precipitation estimates are available at temporal resolutions of 1, 3, 6 and 24 hours and at a spatial resolution of approximately 4km at the equator.

3.4. TRMM Precipitation Product

[17] The combined instrument rain calibration algorithm (3B42) uses combined rain structure and the visible infrared sensor (VIRS) calibration to adjust IR estimates from geosynchronous IR observations [*Huffman et al.*, 1995; *Huffman*, 1997; *Huffman et al.*, 1997]. That is, global precipitation estimates are made by adjusting the GOES Precipitation Index (GPI) [*Arkin and Meisner*, 1987] to the Tropical Rainfall Measuring Mission (TRMM) estimates. The data used in this study are 1-day rainfall estimates on a 1° × 1° grid taken from an original geographic coverage between 40°N and 40°S. The data were acquired as part of

TRMM using algorithms developed by the TRMM science team [*Simpson et al.*, 1996; *Halverson et al.*, 2002; *Petersen et al.*, 2002]. These data, processed by the TRMM Science Data and Information System (TSDIS), are archived and distributed by the NASA Goddard Space Flight Center Distributed Active Archive Center (DAAC).

3.5. Observed Data

[18] Rain gauge data from conventional in situ stations in South America were obtained from local institutes, such as the Brazilian National Institute of Meteorology (INMET) which represents the World Meteorological Organization (WMO) in Brazil, through the databases at CPTEC. The data is in the form of daily average precipitation values for the year 2000. This matched the time period for which Eta model-calculated data were available. In practice, many stations did not report every day in 2000 and only those stations with an adequate yearly reporting record were used in the evaluation. Stations were considered acceptable for use in this evaluation if they reported on a minimum of 300 days. During 2000, of the 998 stations reporting rainfall in South America, only 240 reported on more than 300 days. The distribution of the surface stations used in the product evaluation is shown in Figure 1.

4. Analysis Methods

4.1. Comparison With Observations

[19] The motivation for the present analysis is the evaluation of candidate precipitation products for possible use in the context of a South American LDAS for the CPTEC version of the Eta model. The analysis is based therefore on the grid resolution of that model. The Eta model-derived product is, of course, already available at the 40 km Eta model resolution. The three remotely sensed data products were interpolated to match the model resolution using a general bilinear interpolator function, which is a linear weighted combination of the nearest four pixels in the original data set. These four (now gridded) products were then compared with observations in those grid squares, where at least one observation was available. If more than one observation was available in a grid square, a linear average of the available observations was used in the evaluation.

[20] The year 2000 was found to be the only period where all the products overlapped significantly in time. Although the PERSIANN product was only available for 10 months during this year, the results obtained using it are considered statistically significant for the purposes of this study. As noted in the introduction, to evaluate the utility of the remote sensing products in the context of a potential LDAS, the products should accurately reflect the daily precipitation amounts on any given day, rather than match the daily precipitation in an average or climatological sense. Consequently, the evaluation measures discussed below are all calculated at the daily timescale.

4.2. Evaluation Measures

[21] Measures used to evaluate numerical weather forecasts made with regional models include fractional covered area (FCA), threat score (TS), relative volumetric bias (RVB), root-mean-square error (RMSE) and correlation coefficients [*Anthes*, 1983; *Anthes et al.*, 1989]. All five measures were selected for use in this study. The first three were calculated for the entire study domain as a whole, while the latter two were calculated for three subregions of the South American continent. The correlation coefficients used in this evaluation are spatial correlation coefficients that evaluate the internal structure of the daily precipitation fields.

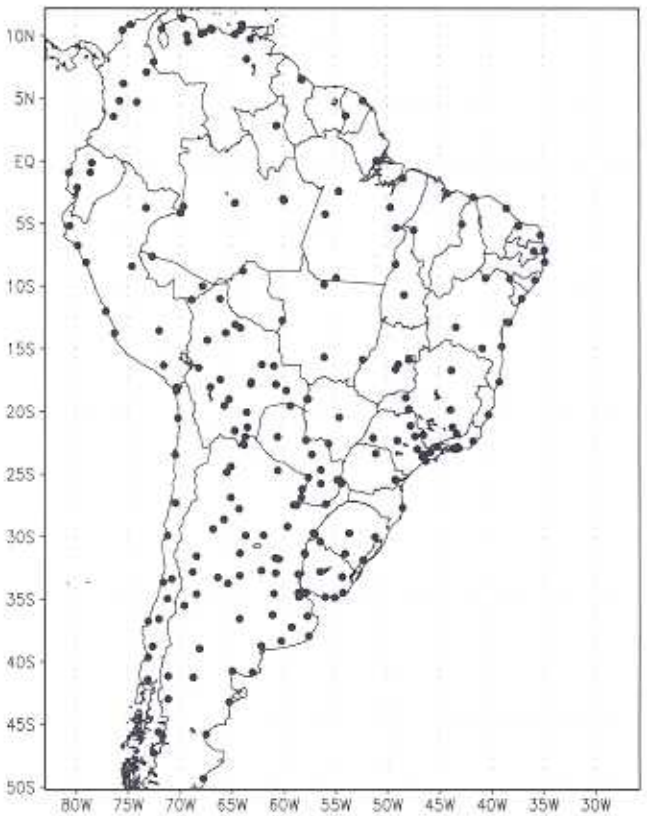

Figure 1. Spatial distribution of the valid surface meteorological stations across continental South America used for this study.

[22] The fractional covered area (FCA) measures the model's tendency to systematically overestimate or underestimate the area of precipitation within a defined domain for a given precipitation threshold. It is defined as

$$\mathrm{FCA} = \frac{F}{O} \tag{1}$$

where F is the number of times that a predicted point precipitation lies above a certain threshold and O is the number of times that an observed point precipitation lies above the same threshold. Consequently, the FCA is above (below) unity when the areal extent of predicted precipitation is greater (less) than the areal extent of observed precipitation above a threshold P. The threat score (TS) measures the model's skill to forecast the area of precipitation for a certain threshold, defined as [e.g., *Anthes et al.*, 1989] as

$$\mathrm{TS} = \frac{H}{F + O - H} \tag{2}$$

where H is the number of "hits", that is, the number of times in which both predicted and observed point precipitation lie above that threshold. It is often used in combination with the FCA. The third measure used in this analysis, the relative volumetric bias (RVB) is the total volume of predicted precipitation error relative to the observed precipitation for a given area. It is defined as

$$\mathrm{RVB} = \frac{1}{N}\sum_{n=1}^{N}\left(\frac{1}{M}\sum_{m=1}^{M}\frac{\mathrm{MOD}_{nm} - \mathrm{OBS}_{nm}}{\mathrm{OBS}_{nm}}\right) \quad (3)$$

where N is the total number of points, M is the total number of days, MOD is the product precipitation value, and OBS is the gauge-based observed value.

[23] The RMSE calculated between each station and predicted values is described as

$$\mathrm{RMSE} = \sqrt{\frac{1}{N}\sum_{n=1}^{N}(X_n - Y_n)^2} \quad (4)$$

where N is the total number of evaluated points, X represents the predicted values and Y the observations. The RMSE was computed for three regions described below for each valid station within the region. The daily RMSE values were then averaged to produce a monthly average value.

[24] To evaluate the spatial distribution of precipitation estimated by each product, the continent was separated in three regions (north, northeast and south) according to the unique rainfall regimes described in section 2. The north (N) region extends from 20°S, 80°W to 10°N, 50°W, the Northeast (NE) from 20°S, 50°W to 10°N, 35°W and south (S) from 55°S, 80°W to 20°S, 40°W. Similar areas have been chosen in previous work in which the Eta CPTEC model performance when simulating precipitation and other fields has been evaluated [*Chou and da Silva*, 1999; *Chou et al.*, 2000, 2003, 2005]. For each region, spatial cross correlation coefficients were computed between each location with a valid rain gauge and surrounding gauges within a radius of 500 km. The cross correlation between two stations is given by

$$r = \frac{\sum_{i=1}^{N}\left[(x_i - \bar{x})(y_{(i-d)} - \bar{y})\right]}{\sqrt{\sum_{i=1}^{N}(x_i - \bar{x})^2}\sqrt{\sum_{i=1}^{N}(y_{(i-d)} - \bar{y})^2}} \quad (5)$$

where x(i) and y(i) are two series with i = 1, 2, ..., N and N the length of the series. A lag time between the series can be defined by d = 1, 2, ..., N-1. For the present study the lag zero correlation (d = 0) was larger than the lagged correlations, which indicates small significance of the storm movement. The lag zero correlation decreased with increasing distance while the lagged correlations did not show significant changes with increasing distance. Because the resulting plots of correlation versus distance are inherently noisy, a decay function was fitted to the point data to facilitate comparison. An exponential function best described decrease in correlation with distance and was used for all cases.

[25] The performance of the several precipitation products (in the form of 24 hour totals prior to 12:00 UTC) was evaluated for the year 2000 according to their ability to represent precipitation amounts, P. The thresholds for the calculation of FCA and TS were taken to be the same as those used for evaluation of the operational Eta model at NCEP, and were equal to $P = 0$ mm, $P > 0$ mm, $P > 5$ mm, $P > 10$ mm, $P > 15$ mm, $P > 20$ mm, $P > 30$ mm, and $P > 50$ mm. Statistical scores were calculated wherever the observations were available.

[26] Fractional covered area, relative volumetric bias, and threat score evaluations were calculated for four successive 90-day periods using these 240 stations. RMSE was calculated for each month for three different subregions, and the spatial correlation was calculated for the entire period for the same three subregions. For a perfect forecast, TS = 1, FCA = 1, RVB = 0, and RMSE = 0.

5. Results

[27] The products were evaluated for the regions of the Eta model domain (continental South America), over the land surface only. The averaged FCA values for the four quarters of the year (January–March, April–June, July–September, and October–December) for the same periods and all threshold levels are presented in Table 1, and the same for TS is presented in Table 2. An example of the 16-day running mean FCA calculated for $P > 5$ mm is given in Figure 2 and an example of the 16-day running mean TS calculated for $P > 5$ mm is given in Figure 3. It is noticeable in Figure 3 that the Eta model has a large seasonal variability while the other remote sensing products show small variation in the skill throughout the year. *Chou and da Silva* [1999] used an objective analysis to evaluate the Eta model precipitation forecasts over South America and found that the lowest TS values occur during the winter, in particular, in the NE region. In that region, the precipitation was systematically underestimated which might be related to deficiencies in the convective parameterization scheme. The model physics have parameters that are strongly dependent on seasons, such as vegetation, albedo, radiative fluxes, etc. Some parameters may need further tuning for winter events.

[28] In Table 1, bold values highlight where FCA reaches its best value (closest to 1) for each threshold and time period. In the first quarter, Eta has the best FCA values for thresholds from P > 0 to P > 20 and NESDIS has the best values for the remaining thresholds (P = 0, P > 30 and P > 50). In the second quarter, Eta has the best values for thresholds of P = 0, P > 0 and P > 10, PERSIANN for P > 5, and NESDIS for P > 15 to P > 50. In the third quarter, Eta has the best FCA values for P = 0 and P > 0, TRMM for P > 5, NESDIS for P > 20 to P > 50, and PERSIANN for P > 10 and P > 15. In the last quarter, Eta has the best FCA values for P > 0, PERSIANN for P > 5, and NESDIS for P = 0 and for P > 10 to P > 50.

[29] In Table 2, bold values highlight where TS reaches its best value for each threshold and time period. A value of TS equal to zero means there is no agreement between observed and predicted values above a certain threshold. For all quarters, TS decreases as the threshold increases,

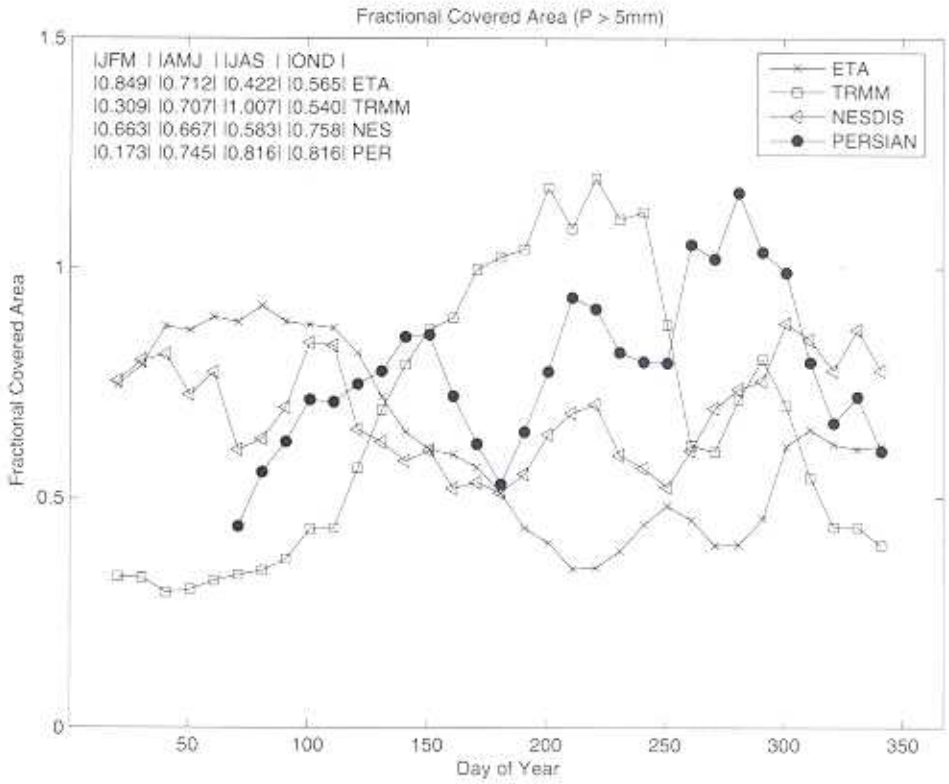

Figure 2. FCA for the 16-day running mean rainfall greater than 5 mm for the ETA, TRMM, NESDIS, and PERSIANN precipitation products as a function of day of the year during 2000. The 90-day average values for 3 month periods are given at the top left.

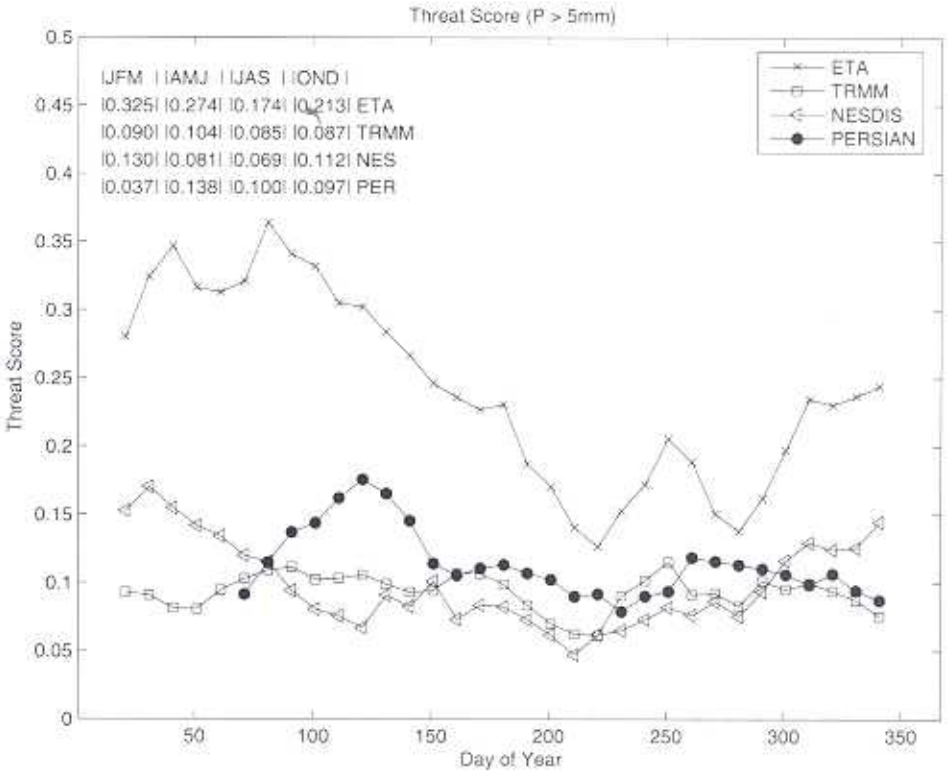

Figure 3. TS for 16-day running mean precipitation greater than 5 mm for the ETA, TRMM, NESDIS, and PERSIANN precipitation products as a function of day of the year during 2000. The 90-day average values for 3 month periods are given at the top left.

Table 1. Average Fractional-Covered Area (Equation (1)) for the Four Time Periods in 2000 for Each of the Eight Thresholds P (Including Zero Rainfall)[a]

	ETA	TRMM	NESDIS	PERSIANN
		January–March		
P = 0 n = 137	0.850	0.721	**1.029**	0.249
P > 0 n = 101	**1.085**	1.279	0.872	0.471
P > 5 n = 67	**0.849**	0.309	0.663	0.173
P > 10 n = 54	**0.686**	0.111	0.493	0.113
P > 15 n = 48	**0.504**	0.029	0.382	0.066
P > 20 n = 45	**0.324**	0.005	0.301	0.043
P > 30 n = 40	0.088	0.000	**0.216**	0.023
P > 50 n = 36	0.002	0.000	**0.122**	0.004
		April–June		
P = 0 n = 154	**1.000**	0.339	1.072	0.721
P > 0 n = 85	**0.933**	2.586	0.848	1.716
P > 5 n = 50	0.712	0.707	0.667	**0.745**
P > 10 n = 39	**0.573**	0.279	0.522	0.563
P > 15 n = 34	0.405	0.091	**0.431**	0.403
P > 20 n = 32	0.262	0.030	**0.362**	0.276
P > 30 n = 27	0.097	0.004	**0.297**	0.131
P > 50 n = 25	0.003	0.000	**0.213**	0.029
		July–September		
P = 0 n = 163	**1.008**	0.327	1.076	0.657
P > 0 n = 76	**0.735**	2.933	0.704	1.975
P > 5 n = 43	0.422	**1.007**	0.583	0.816
P > 10 n = 34	0.255	0.517	0.467	**0.614**
P > 15 n = 30	0.145	0.237	0.388	**0.461**
P > 20 n = 28	0.063	0.095	**0.338**	0.336
P > 30 n = 25	0.013	0.006	**0.282**	0.183
P > 50 n = 23	0.001	0.000	**0.215**	0.055
		October–December		
P = 0 n = 145	0.983	0.509	**1.025**	0.563
P > 0 n = 94	**0.967**	2.193	0.941	2.135
P > 5 n = 61	0.565	0.540	0.758	**0.816**
P > 10 n = 50	0.366	0.241	**0.664**	0.586
P > 15 n = 46	0.211	0.105	**0.583**	0.408
P > 20 n = 43	0.122	0.042	**0.510**	0.289
P > 30 n = 39	0.030	0.013	**0.366**	0.145
P > 50 n = 36	0.002	0.000	**0.240**	0.040

[a]Here n is the number of observations. Bold values highlight the highest value for each threshold and time period.

reaching zero or approximately zero in some cases. In the first and second quarters, Eta has the best TS for all thresholds except for P > 50 where NESDIS yielded a marginally better value (0.014 for both quarters). In the third quarter, Eta has the best values for thresholds from P = 0 to P > 15, PERSIANN for P > 20 and P > 30, and NESDIS for P > 50. In the last quarter, Eta has the best TS values for P = 0 to P > 15 and NESDIS for P > 20 to P > 50. Zero values of TS are found for Eta (third quarter, P > 50) and TRMM (all quarters for P > 50, and third quarter for P > 30). In general, all three satellite derived products (TRMM, NESDIS, and PERSIANN) have TS values less than 0.1 in all quarters for thresholds above P > 10.

[30] Figure 4 shows the zonal precipitation over continental South America normalized by the land area in each longitude band. Precipitation for oceanic grid squares is not included in the average. Figure 4 (left) shows the mean zonal precipitation, while Figure 4 (right) shows the relative volumetric bias (RVB) expressed as a percentage. The products were evaluated for the four quarters of the year as well as for the whole year. The mean zonal observed precipitation shows maximum values (around 10 mm/day) in the north of the continent during the first and second quarters, with progressively less rainfall as the latitude increases southward. During the third and fourth quarters, the mean zonal precipitation throughout the continent is around 5 mm/day. The Eta model precipitation estimates follow the observed pattern with a maximum in the first and second quarters of around 15 mm/day in the north and less than observed (near zero rainfall) in the south (>20°S). The NESDIS product overestimates precipitation at all locations in all quarters except in the north (<10°S) in the first semester. In the third trimester, the NESDIS product overestimates precipitation in the south (up to 15 mm/day) and central areas (10°–30°S) by approximately 5 mm/day. The TRMM product underestimates observations in the first and second quarters by up to 5 mm/day in the north of the continent and PERSIANN shows its maximum difference in the third quarter of 4 mm/day around 10°S. The annual mean zonal precipitation shows differences up to 2 mm/day between all products and observations except NESDIS that shows differences up to 5 mm/day in the southern areas and around 10°N. The Eta model product also shows the same 5 mm/day difference at 10°N.

Table 2. Average Threat Score (Equation (2)) for the Four Time Periods in 2000 for Each of the Eight Thresholds P (Including Zero Rainfall)[a]

	ETA	TRMM	NESDIS	PERSIANN
		January–March		
P = 0 n = 137	**0.612**	0.408	0.531	0.123
P > 0 n = 101	**0.396**	0.225	0.165	0.070
P > 5 n = 67	**0.325**	0.090	0.130	0.037
P > 10 n = 54	**0.241**	0.032	0.087	0.022
P > 15 n = 48	**0.178**	0.009	0.063	0.014
P > 20 n = 45	**0.116**	0.001	0.049	0.009
P > 30 n = 40	**0.032**	0.001	0.030	0.005
P > 50 n = 36	0.001	0.000	**0.014**	0.001
		April–June		
P = 0 n = 154	**0.712**	0.222	0.592	0.459
P > 0 n = 85	**0.390**	0.242	0.139	0.241
P > 5 n = 50	**0.274**	0.104	0.081	0.138
P > 10 n = 39	**0.194**	0.042	0.046	0.086
P > 15 n = 34	**0.133**	0.014	0.032	0.054
P > 20 n = 32	**0.086**	0.006	0.026	0.042
P > 30 n = 27	**0.024**	0.001	0.020	0.016
P > 50 n = 25	0.001	0.000	**0.014**	0.004
		July–September		
P = 0 n = 163	**0.713**	0.211	0.655	0.450
P > 0 n = 76	**0.293**	0.182	0.117	0.211
P > 5 n = 43	**0.174**	0.085	0.069	0.100
P > 10 n = 34	**0.093**	0.043	0.040	0.063
P > 15 n = 30	**0.051**	0.020	0.029	0.046
P > 20 n = 28	0.027	0.011	0.022	**0.030**
P > 30 n = 25	0.004	0.001	0.013	**0.014**
P > 50 n = 23	0.000	0.000	**0.005**	0.004
		October–December		
P = 0 n = 145	**0.693**	0.316	0.576	0.343
P > 0 n = 94	**0.342**	0.213	0.136	0.206
P > 5 n = 61	**0.213**	0.087	0.112	0.097
P > 10 n = 50	**0.129**	0.034	0.084	0.058
P > 15 n = 46	**0.072**	0.012	0.066	0.035
P > 20 n = 43	0.038	0.005	**0.055**	0.023
P > 30 n = 39	0.008	0.000	**0.039**	0.010
P > 50 n = 36	0.001	0.000	**0.020**	0.002

[a]Here n is the number of observations. Bold values highlight the highest value for each threshold and time period.

[31] Figure 4 (right) shows the RVB, which is a measure of the estimated total zonal precipitation relative to observations. If RVB = 0%, there is perfect agreement between estimated and observed total zonal precipitation (equation (3)). NESDIS shows the highest RVB values for all quarters for latitudes south of 10°S, with values above 100%, reaching peaks of 600% in the second and fourth quarters, and more than 600% in the third quarter. In the third quarter, PERSIANN shows values up to 600% around 30°S and more than 200% for latitudes greater than 30°S. All the products except TRMM show an annual average peak of up to 600% for latitudes north of 5N.

[32] South of 5°N, all the products oscillate between −50% and 50%, but NESDIS reaches values of up to 250% at 40°S in the annual average RVB.

[33] The monthly averaged RMSE is shown in Figure 5 for each month. The vertical bars illustrate the standard deviation computed for each month. Because the standard deviation (and RMSE) of the NESDIS product is high compared to the other products, its results are plotted separately on the right with a different scale. In the northern region (N), the RMSE of PERSIANN, when available, is around 10 mm/day. For the period January to June, TRMM has the lowest RMSE, on average about 1 mm/day less than Eta. From July to December, Eta has the lowest RMSE, which is on average 2 mm/day less than TRMM. The maximum RMSE for TRMM and Eta occur in February (8 mm/day and 8.9 mm/day, respectively), for PERSIANN in September (11.5 mm/day), and NESDIS in July (20 mm/day). The minimum RMSE for TRMM, Eta, and PERSIANN occur in August (5 mm/day, 3.5 mm/day, and 9.1 mm/day, respectively) and for NESDIS in September (7.7 mm/day).

[34] In the northeastern region (NE), the RMSE of PERSIANN, when available, is around 10 mm/day. For the months January to June, TRMM has the lo west RMSE (as for the northern region), followed by Eta. The differences between TRMM and Eta during this period are less than 1 mm/day). From July to December, Eta has the lowest RMSE (again as for the northern region), followed by TRMM. The differences between TRMM and Eta during this period are less than 2 mm/day. The maximum RMSE for TRMM, Eta, and PERSIANN occur in April (8.2 mm/day, 9 mm/day, and 11.2 mm/day respectively), and for

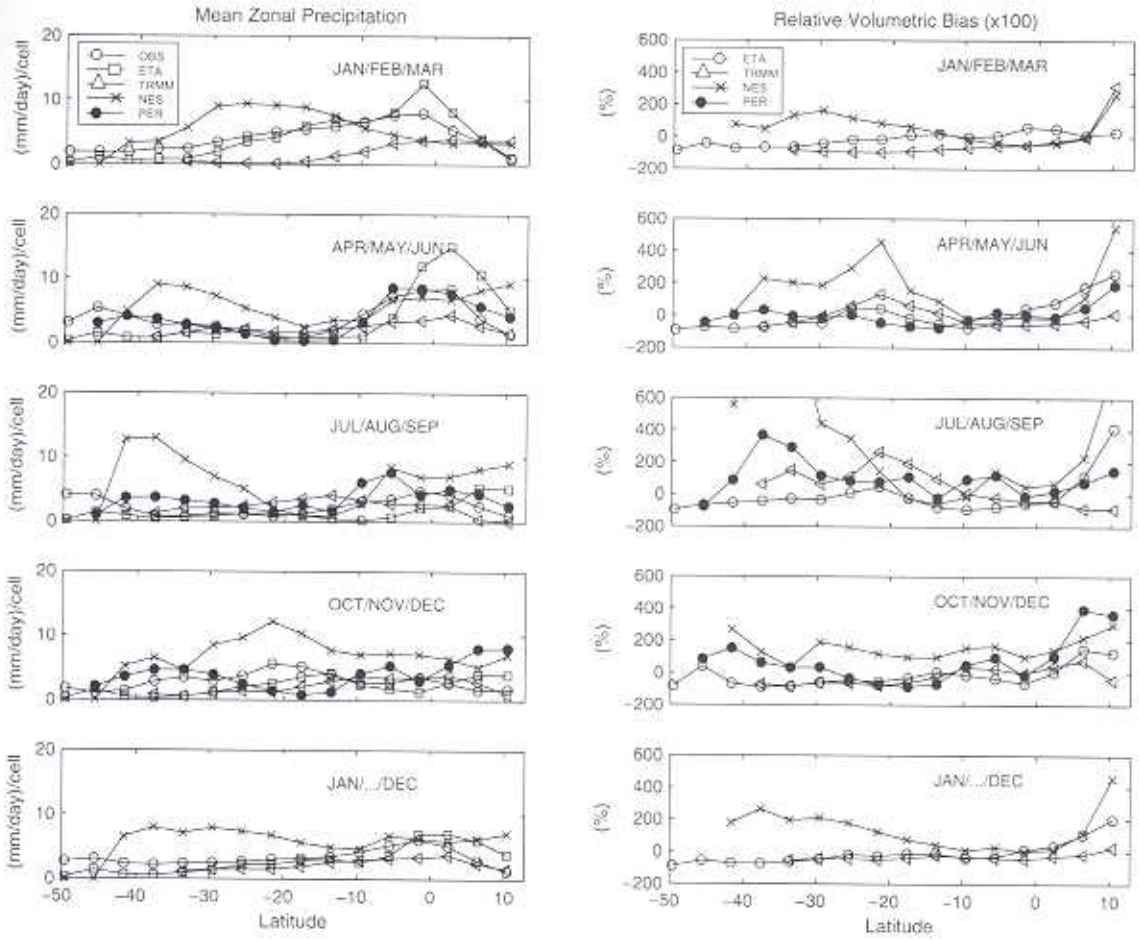

Figure 4. (left) Zonal average precipitation over continental South America for the ETA, TRMM, NESDIS, and PERSIANN precipitation products and the observations. (right) Relative volumetric bias. Data are shown for four quarters of the year as well as the whole year.

NESDIS in July (22 mm/day). The minimum RMSE for TRMM, Eta, PERSIANN and NESDIS all occur in August (5.2 mm/day, 3.3 mm/day, 8.5 mm/day, and 8.0 mm/day, respectively). In the southern region (S), the TRMM product has the lowest RMSE for the entire period, followed in order by Eta, PERSIANN, and NESDIS. The average difference between TRMM and Eta is 1.3 mm/day, with the minimum difference in June (0.5 mm/day) and maximum difference in July (2.4 mm/day). The maximum RMSE values for TRMM, Eta, and PERSIANN occur in December (8.5 mm/day, 7.4 mm/day, and 10.4 mm/day, respectively) and for NESDIS in November (20 mm/day). The minimum RMSE values for TRMM and Eta occur in July (5.2 mm/day and 2.8 mm/day, respectively), PERSIANN in May (7.0 mm/day), and NESDIS in January (8.8 mm/day). For the three regions analyzed, the observations show that the cross correlation coefficients decrease with distance. Figure 6a shows the calculated correlation coefficients versus distance, with fitted curves for the observations (blue) and PERSIANN (red) products given as examples. Comparisons between the fitted curves, based on an exponential decay function, are shown in Figures 6b, 6c, and 6d for the NE, N, and S regions, respectively. In the NE region (Figure 6b), the fitted curve for PERSIANN (dashed line) matches the observations most closely. This is followed, in decreasing order, by Eta (circles), TRMM (crosses), and NESDIS (dots). For the N region (Figure 6c), this pattern is repeated. Figure 6d shows the comparison for S region. In this case, NESDIS shows better agreement with the observations for distances less 200 km. Eta and TRMM yield very similar curves which most similar to observations for distances greater than 200 km.

6. Discussion

[35] When considering the potential value of a precipitation product for use in an LDAS, aspects that merit special consideration are a tendency to overestimate or underestimate precipitation amount (bias), the degree to which the spatial structure of the observations is captured, and the performance when estimating zero or high-intensity rainfall. For all threshold $P > 5$ mm/day and greater, all four precipitation products have an FCA value less than one, that is, the area estimated to have rainfall is less than observed. This may result, in part, from our method of comparison, in which grid-averaged products are compared with observations from individual gauges. The Eta model and NESDIS product are approximately equally successful

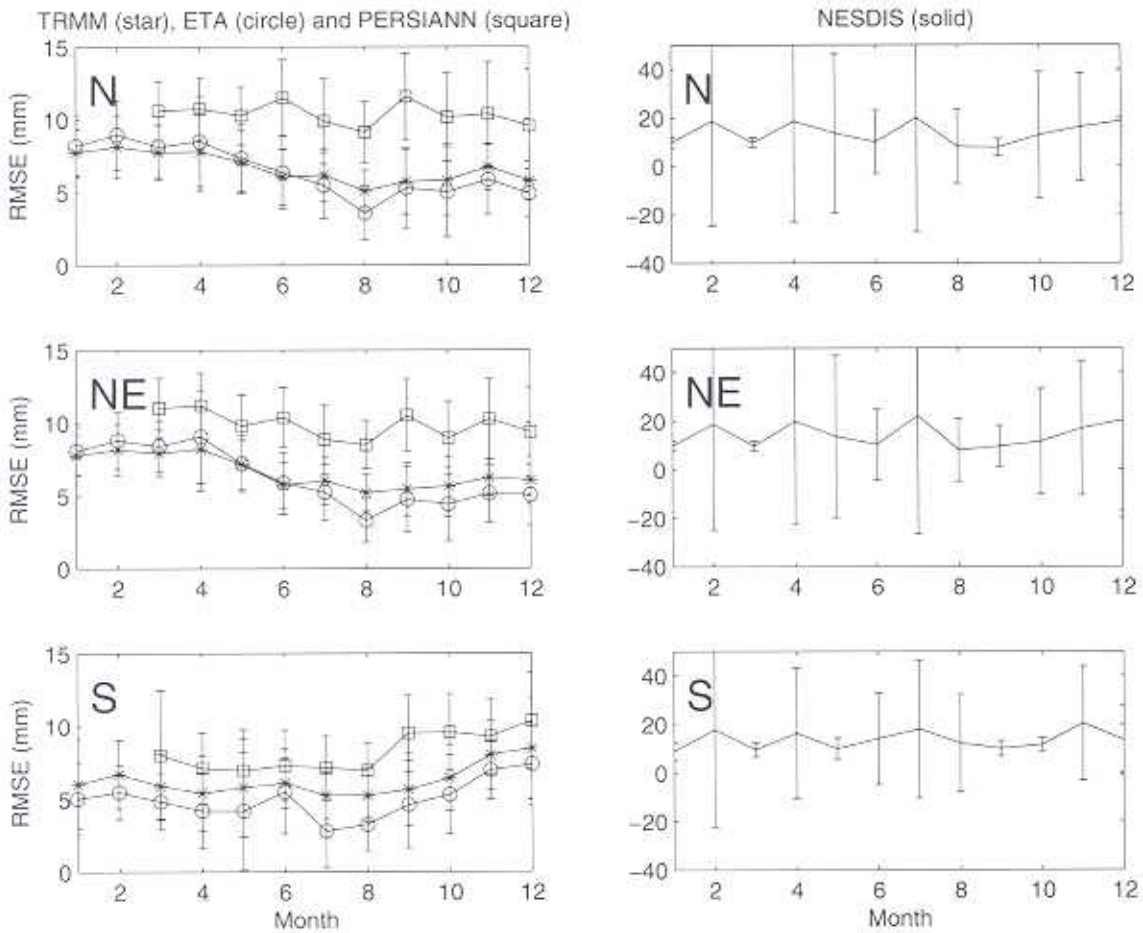

Figure 5. TRMM, ETA, PERSIANN and NESDIS rainfall monthly averaged RMSE for N, NE, and S regions in mm. The vertical bars show the standard deviation for each month (NESDIS is plotted in a separate column because of its high standard deviation relative to the others).

in terms of FCA and capture the area without precipitation within the domain reasonably well, although their relative success in doing so changes through the year. The TRMM and PERSIANN products tend to underestimate the area without precipitation and to heavily overestimate the area with a small amount of precipitation (less than 5 mm/day). It is interesting that the NESDIS and PERSIANN products, which are both GOES-derived products, show different behavior with respect to FCA, not only in terms of their annual average values, but also in terms of its variation with time of year.

[36] All of the precipitation products have low values of TS (less than 0.6, in general) if precipitation is greater than zero. For high precipitation intensity thresholds ($P >$ 20 mm/day), values of TS are typically less than 0.1. The Eta model-derived product gives noticeably better TS for all but the highest rainfall threshold. It is better in 80% of the cases, and much better when P = 0 mm/day. The NESDIS product has the highest TS for areas with very heavy precipitation (P > 50 mm/day), but its TS for heavy precipitation is nonetheless very low although there are few eve nts for that threshold. The TRMM product underestimates precipitation, with the domain average precipitation for this product being 2.2 mm/day/cell, while the NESDIS product significantly overestimates precipitation, the domain average precipitation being 5.8 mm/day/cell.

[37] In terms of zonal behavior, the Eta model-derived precipitation product broadly follows the pattern of observations, but it significantly overestimates the peak of precipitation between 10°S and 10°N. For latitudes below 10°S, the zonal average Eta product correlates quite well with observations in the first half of the year, but in the second half of 2000 the peak in the zonal average Eta product is north of that for observations (at about 10°N), and the correlation below 10°S is less good. The TRMM product noticeably underestimates precipitation through most of the year (except in the period October to December). In general, the NESDIS product significantly overestimates precipitation.

[38] Over the 10 months for which predictions are available, the PERSIANN product shows reasonably good average agreement, but it overestimates precipitation for latitudes north of 15°S and south of 25°S. The domain average of the observations is 3.3 mm/day (the domain only includes cells which contain one or more stations). The Eta model-calculated data and PERSIANN product broadly match the domain average observations, with domain averages of 3.07 mm/day and 3.67 mm/day respectively. In the

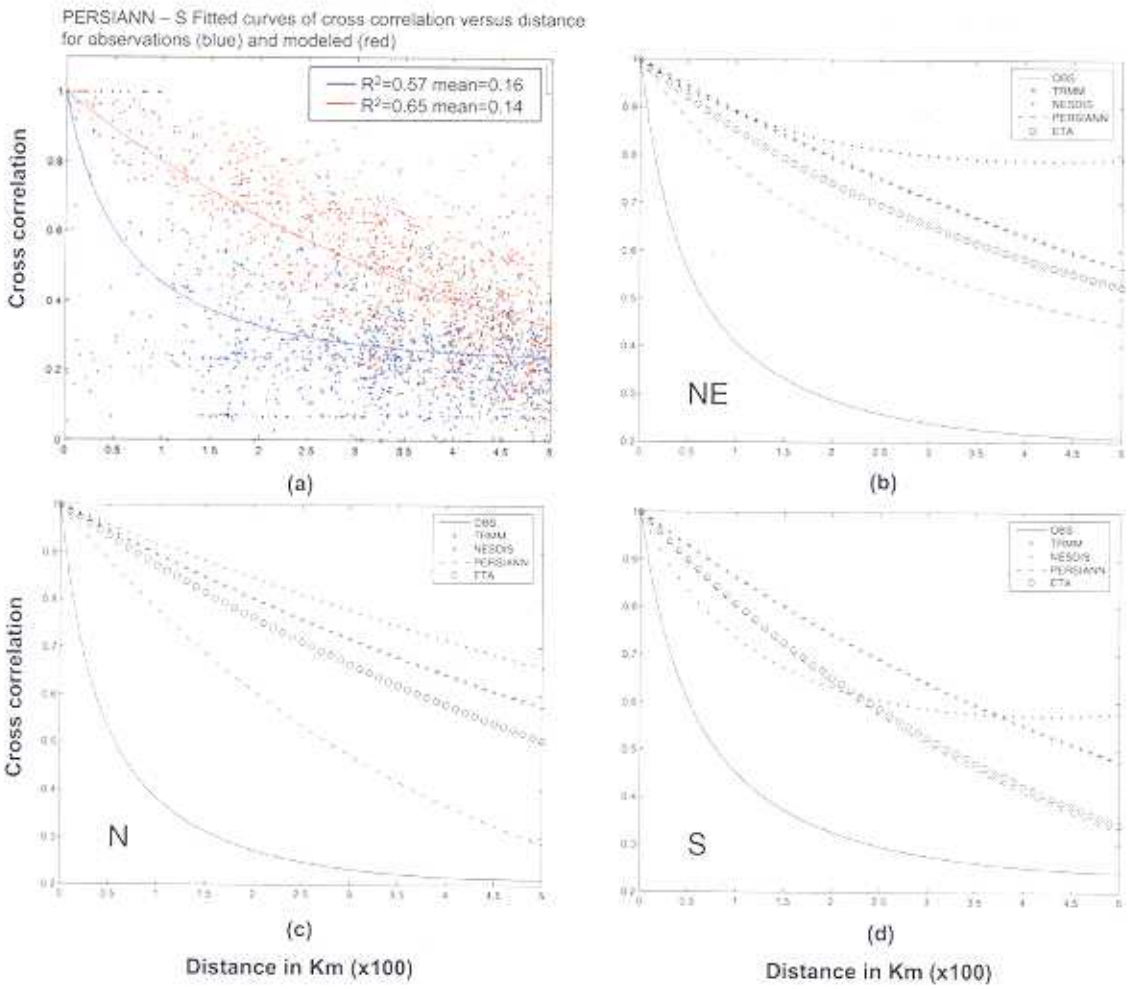

Figure 6. Cross-correlation coefficient versus distance for each valid location within each region: (c) north, (b) northeast, and (d) south. (a) Example of the data distribution and the fitted curve for PERSIANN and observations. The x axis represents the distance in hundreds of kilometers, and the y axis represents the cross-correlation coefficient.

second and third quarters, the NESDIS product has two zones with strong precipitation; one near the Equator and one at about 30°S. The TRMM product and the NESDIS product show domain averages of 2.2 mm/day and 5.8 mm/day, respectively.

[39] In terms of RMSE, TRMM and Eta are the best products for the N and NE regions. NESDIS shows the highest RMSE values in all regions for the whole period studied. In the S region, the Eta model has the lowest RMSE for the whole period.

7. Summary and Conclusions

[40] The fractional covered area (FCA) determines whether the product overestimates or underestimates the area of precipitation. This is often used in conjunction with the threat score (TS), which measures the model's ability to forecast the location of events. The relative volumetric bias (RVB), measures the total volume of predicted precipitation relative to that observed. The RMSE gives a measure of the absolute value of the departure from the observation, while the distribution of cross correlation coefficients with distance measures the model ability to reproduce the spatial structure of precipitation. These measures were used in conjunction with available observations of daily total rainfall across South America to evaluate four precipitation products: the 6 hour predictions from the CPTEC Eta model, and three different satellite-derived estimates of precipitation (PERSIANN, NESDIS, and TRMM).

[41] In a LDAS context, precipitation generated by the atmospheric model is used, along with other forcing information, by the LSM to create a background field of land surface states. Remote sensed information along with sparse surface data are then assimilated to correct inherent systematic errors in the land surface states errors in the atmospheric model. Thus in this study, the above mentioned characteristics of precipitation are analyzed and compared between the Eta model and three precipitation products to determine whether weaknesses of the former could be addressed by the latter. It is important to remember that the analysis presented here is for only for 1 year (2000) and the number of stations with sufficient observations is limited. However, to be useful in an LDAS context, the precipitation products should reflect as accurately as possible spatially distributed precipitation on any given day. This is a stricter and more challenging requirement than matching the observed pre-

cipitation in some average or climatological sense, and this has been the focus of the present study.

[42] The Eta model-calculated data and NESDIS product are broadly comparable in terms of success in defining the fractional covered area of the domain with precipitation, the Eta model data being better for low precipitation thresholds and the NESDIS product for high precipitation threshold. However, the comparative success of the NESDIS product in terms of fractional coverage area for high precipitation thresholds may just be a consequence of its tendency to heavily overestimate precipitation in general. The NESDIS product is also the most successful at identifying the location of areas with very heavy precipitation ($P > 50$ mm), although it is still relatively poor. The Eta model-calculated precipitation and PERSIANN product broadly match the zonal average observations. However, both tend to bias the zonal location of precipitation toward the Equator more than the observations. The PERSIANN product also tends to underestimate the area without precipitation, to overestimate the area with a small amount of precipitation (less than 5 mm), and has difficulty locating areas with and without precipitation. The TRMM product underestimates overall precipitation and does not capture the location of precipitation and the fractional area with precipitation as efficiently as the other products.

[43] In general, the Eta model-calculated precipitation outperforms the remotely sensed products evaluated in the present study in that it provides the best agreement with both the overall observed amount of precipitation and the observed location of precipitation. However, some specific features merit mention.

[44] 1. The TRMM product has a regional RMSE similar to Eta.

[45] 2. PERSIANN has a better spatial distribution of precipitation cross correlation coefficients than Eta in the N and NE areas. This suggests that PERSIANN could better explain the evolution of precipitation systems in these regions (e.g., squall lines)

[46] 3. TRMM and NESDIS also have better spatial distribution of correlation coefficients in the S region, which could be related to mesoscale convective complex development and the frontal systems that are characteristics of this region.

[47] 4. In the case of FCA, NESDIS outperforms Eta for high precipitation thresholds, and the differences are small where Eta outperforms NESDIS.

[48] In South America and other locations where surface observations of precipitation are sparse, remotely sensed products could potentially be a promising source of information. However, the Eta model-produced precipitation fields compared better with gauge observations than with any of the four remote-sensing-based products evaluated in this study, though none of the observations used for the comparison were assimilated by the model. From an LDAS application point of view this is problematic because it is exactly these model fields (i.e., Eta model fields) one would like to improve. At this time, there may be an opportunity to correct some of the weaknesses in the Eta product by developing a combined Eta remote-sensing product, but significant improvements in remotely sensed precipitation fields are necessary before they will be of real use in an LDAS context.

[49] **Acknowledgments.** Primary support for this research came from NASA project NAG5-9796. Additional support for W. James Shuttleworth and Eleanor Burke came from NASA project NAG5-8214. The authors wish to acknowledge the help of the staff at CPTEC in making the Eta model-calculated data available. The editorial assistance provided by Corrie Thies is greatly appreciated. Portions of the data used in this study were acquired as part of the Tropical Rainfall Measuring Mission (TRMM). The algorithms were developed by the TRMM science team. The data were processed by the TRMM Science Data and Information System (TSDIS) and the TRMM Office; they are archived and distributed by the Goddard Distributed Active Archive Center (DAAC). TRMM is an international project jointly sponsored by the Japan National Space Development Agency (NASDA) and the U.S. National Aeronautics and Space Administration (NASA) Office of Earth Sciences. The authors also wish to acknowledge the Hydrological Sciences Branch, Code 614.3, at NASA GSFC and the NASA Postdoctoral Program.

References

Anthes, R. A. (1983), Regional models of the atmosphere in middle latitudes, *Mon. Weather Rev., 111*, 1306–1335.

Anthes, R. A., Y.-H. Kuo, E.-Y. Hsie, S. Low-Nam, and T. W. Bettge (1989), Estimation of skill and uncertainty in regional numerical models, *Q.J.R. Meteorol. Soc., 115*, 763–806.

Arkin, P. A., and B. N. Meisner (1987), The relationship between large-scale convective rainfall and cold cloud over the Western Hemisphere during 1982–84, *Mon. Weather Rev., 115*, 51–74.

Beljaars, A. C. M., P. Viterbo, M. J. Miller, and A. K. Betts (1993), Anomalous rainfall over the U.S. during July 1993: Sensitivity to land surface parameterization, *Mon. Weather Rev., 124*, 364–383.

Betts, A. K., and M. J. Miller (1986), A new convective adjustment scheme, part II: Single column model tests using GATE wave, BOMEX, and Arctic air-mass data sets, *Q. J. R. Meteorol. Soc., 112*, 693–709.

Betts, A. K., J. H. Ball, A. C. M. Beljaars, M. J. Miller, and P. Viterbo (1996), The land-surface-atmosphere interaction: A review based on observational and global modeling perspectives, *J. Geophys. Res., 101*, 7209–7225.

Black, T. L. (1994), NMC notes: The new NMC mesoscale Eta model: Description and forecast examples, *Weather Forecast., 9*, 256–278.

Bonatti, J. P. (1996), Modelo de circulação geral atmosférico do CPTEC, in *Climanálise Especial (10 anos Edicao Especial)*, 5 pp., Cent. de Previsão de Tempo e Estud. Climáticos, Cachoeira Paulista, Brazil. (Available at http://tucupi.cptec.inpe.br/products/climanalise/cliesp10a/bonatti.html)

Cavalcanti, I. F. A., et al. (2002), Global climatological features in a simulation using the CPTEC-COLA AGCM, *J. Clim., 15*(21), 2965–2988.

Chou, S. C., and M. G. J. da Silva (1999), An objective evaluation of Eta model precipitation forecasts over South America, *Climanalise, 14*, 17 pp.

Chou, S. C., A. M. B. Nunes, and I. F. A. Cavalcanti (2000), Extended range forecasts over South America using the regional Eta model, *J. Geophys. Res., 105*, 10,147–10,160.

Chou, S. C., C. A. S. Tanajura, Y. Xue, and C. A. Nobre (2003), Validation of the Coupled Eta/SSiB Model over South America, *J. Geophys. Res., 107*(D20), 8088, doi:10.1029/2000JD000270.

Chou, S. C., J. Bustamante, and J. Gomes (2005), Evaluation of Eta model seasonal precipitation forecasts over South America, *Nonlinear Processes Geophys., 12*, 537–555.

Dorman, J. L., and P. J. Sellers (1989), A global climatology of albedo, roughness length and stomatal resistance for atmospheric general circulation models as represented by the simple biosphere model (SiB), *J. Appl. Meteorol., 28*, 833–855.

Fast, J. D., and M. D. McCorkle (1991), The effects of heterogeneous soil moisture on a summer baroclinic circulation in the central United States, *Mon. Weather Rev., 119*, 2140–2167.

Fels, S. B., and M. D. Schwarzkopf (1975), The simplified exchange approximation: A new method for radiative transfer calculations, *J. Atmos. Sci., 32*, 1475–1488.

Fennessey, M. J., and J. Shukla (1999), Impact of initial soil wetness on seasonal atmospheric prediction, *J. Clim., 12*, 3167–3180.

Figueroa, S. N., and C. A. Nobre (1990), Precipitation distribution over central and western tropical South America, *Climanalise, 5*, 35–46.

Gadd, J. (1978), A split-explicit integration scheme for numerical weather prediction, *Q. J. R. Meteorol. Soc., 104*, 569–582.

Garreaud, R. D. (2000), Cold air incursions over subtropical South America: Mean structure and dynamics, *Mon. Weather Rev., 128*, 2544–2559.

Halverson, J. B., T. Rickenbach, B. Roy, H. Pierce, and E. Williams (2002), Environmental characteristics of convective systems during TRMM-LBA, *Mon. Weather Rev., 130*, 1493–1509.

Hsu, K., X. Gao, S. Sorooshian, and H. Gupta (1997), Precipitation estimation from remotely sensed information using artificial neural networks, *J. Appl. Meteorol., 36*(9), 1176–1190.

Huffman, G. J. (1997), Estimates of root-mean-square random error for finite samples of estimated precipitation, *J. Appl.*, 1191–1201.

Huffman, G. J., R. F. Adler, B. Rudolph, U. Schneider, and P. Keehn (1995), Global precipitation estimates based on a technique for combining satellite-based estimates, rain gauge analysis, and NWP model precipitation information, *J. Clim.*, *8*, 1284–1295.

Huffman, G. J., R. F. Adler, P. Arkin, A. Chang, R. Ferraro, A. Gruber, J. Janowiak, A. McNab, B. Rudolph, and U. Schneider (1997), The Global Precipitation Climatology Project (GPCP) combined precipitation dataset, *Bull. Am. Meteorol. Soc.*, *78*, 5–20.

Janjic, Z. I. (1979), Forward-backward scheme modified to prevent two-grid-interval noise and its application in sigma coordinate models, *Contrib. Atmos. Phys.*, *52*, 69–84.

Janjic, Z. I. (1984), Non-linear advection schemes and energy cascade on semi-staggered grids, *Mon. Weather Rev.*, *112*, 1234–1245.

Janjic, Z. I. (1994), The step-mountain Eta coordinate model: Further developments of the convection, viscous sub-layer and turbulence closure schemes, *Mon. Weather Rev.*, *122*, 927–945.

Janjic, Z. I. (1996a), The Mellor-Yamada level 2.5 scheme in the NCEP Eta model, paper presented at Eleventh Conference on Numerical Weather Prediction, Am. Meteorol. Soc., Norfolk, Va.

Janjic, Z. I. (1996b), The surface layer in the NCEP Eta model, paper presented at Eleventh Conference on Numerical Weather Prediction, Am. Meteorol. Soc., Norfolk, Va.

Koster, R. D., and M. J. Suarez (1999), A simple framework for examining the interannual variability of land surface moisture fluxes, *J. Clim.*, *12*, 1911–1917.

Koster, R. D., M. J. Suarez, P. Liu, U. Jambor, M. Kistler, A. Berg, R. Reichle, M. Rodell, and J. Famiglietti (2004), Realistic initialization of land surface states: Impacts on subseasonal forecast skill, *J. Hydrometeorol.*, *5*, 1049–1063.

Lacis, A. A., and J. E. Hansen (1974), A parameterization of the absorption of solar radiation in the Earth's atmosphere, *J. Atmos. Sci.*, *31*, 118–133.

Legates, D., and C. Wilmott (1990), Mean seasonal and spatial variability in gauge corrected, global precipitation, *Int. J. Climatol.*, *10*, 111–127.

Liebmann, B., G. Kiladis, J. Marengo, T. Ambrizzi, and J. Glick (1999), Submonthly convective variability over South America and the South Atlantic Convergence Zone, *J. Clim.*, *10*, 1877–1891.

Marengo, J. (1995), Interannual variability of deep convection in the tropical South American sector as deduced from ISCCP C2 data, *Int. J. Climatol.*, *15*, 995–1010.

Marengo, J., and C. Nobre (2001), General characteristics and variability of climate in the Amazon Basin and its links to the global climate system, in Biogeochemistry of the Amazon Basin, edited by V. R. McClaine and J. E. Richey, pp. 17–42, Oxford Univ. Press, New York.

Marengo, J., A. Cornejo, P. Satymurty, C. Nobre, and W. Sea (1997), Cold surges in tropical and extratropical South America: The strong event in June 1994, *Mon. Weather Rev.*, *125*, 2759–2786.

Marengo, J. A., M. W. Douglas, and P. L. Silva Dias (2002), The South American low-level jet east of the Andes during the LBA-TRMM and WET AMC campaign of January–April 1999, *J. Geophys. Res.*, *107*(D20), 8079, doi:10.1029/2001JD001188.

Marengo, J. A., W. R. Soares, C. Saulo, and M. Nicolini (2004), Climatology of the low-level jet east of the Andes as derived from the NCEP-NCAR reanalysis: Characteristics and temporal variability, *J. Clim.*, *17*, 2261–2280.

Maurer, E. P., A. W. Wood, J. C. Adam, D. P. Lettenmaier, and B. Nijssen (2002), A long-term hydrologically based dataset of land surface fluxes and states for the conterminous United States, *J. Clim.*, *15*, 3237–3251.

Mesinger, F. (1984), A blocking technique for representation of mountains in atmospheric models, *Riv. Meteorol. Aeronaut.*, *44*, 195–202.

Mesinger, F., Z. I. Janjic, S. Nickovic, D. Gavrilov, and D. G. Deaven (1988), The step-mountain coordinate: Model description and performance for cases of Alpine lee arelogenesis and for a case of an Appalachian redevelopment, *Mon. Weather Rev.*, *116*, 1493–1518.

Mitchell, K., et al. (2000), The collaborative GCIP Land Data Assimilation System (LDAS) project and supportive NCEP uncoupled land-surface model initiatives, paper presented at 15th Conference on Hydrology, Am. Meteorol. Soc., Long Beach, Calif.

Mitchell, K. E., et al. (2004), The multi-institution North American Land Data Assimilation System (NLDAS): Utilizing multiple GCIP products and partners in a continental distributed hydrological modeling system, *J. Geophys. Res.*, *109*, D07S90, doi:10.1029/2003JD003823.

New, M., M. Todd, M. Hulme, and P. Jones (2001), Precipitation measurements and trends in the twentieth century, *Int. J. Clim.*, *21*, 1889–1922.

Nogués-Paegle, J., and K.-C. Mo (1997), Alternating wet and dry conditions over South America during summer, *Mon. Weather Rev.*, *125*, 279–291.

Peterson, T. C., et al. (1998), Homogeneity adjustments of in situ atmospheric climate data: A review, *Int. J. Climatol.*, *18*, 1493–1517.

Petersen, W. A., S. W. Nesbitt, R. J. Blakeslee, R. Cifelli, P. Hein, and S. A. Rutledge (2002), TRMM observations of intraseasonal variability in convective regimes over the Amazon, *J. Clim.*, *15*, 1278–1294.

Rao, V. B., and K. Hada (1990), Characteristics of rainfall over Brazil: Annual variations and connections with the Southern Oscillation, *Theor. Appl. Climatol.*, *42*, 81–91.

Reynolds, R. W., and T. M. Smith (1994), Improved global sea surface temperature analyses, *J. Clim.*, *7*, 929–948.

Rodell, M., et al. (2004), The Global Land Data Assimilation System, *Bull. Am. Meteorol. Soc.*, *85*, 381–394.

Sellers, P. J., Y. Mintz, Y. C. Sud, and A. Dalcher (1986), A simple biosphere model (SiB) for use within general circulation models, *J. Atmos. Sci.*, *43*, 505–531.

Seluchi, M. E., and J. A. Marengo (2000), Tropical-midlatitude exchange of air masses during summer and winter in South America: Climatic aspects and examples of intense events, *Int. J. Climatol.*, *20*, 1167–1190.

Simpson, J., C. Kummerow, W. K. Tao, and R. F. Adler (1996), On the Tropical Rainfall Measuring Mission (TRMM), *Meteorol. Atmos. Phys.*, *60*, 19–36.

Velazco, I., and J. M. Fritsch (1987), Mesoscale convective complexes in the Americas, *J. Geophys. Res.*, *92*, 9591–9613.

Vicente, G. A., R. A. Scofield, and W. P. Menzel (1998), The operational GOES infrared rainfall estimation technique, *Bull. Am. Meteorol. Soc.*, *79*, 1883–1898.

Willmott, C. J., C. M. Rowe, and Y. Mintz (1985), Climatology of the terrestrial seasonal water cycle, *J. Climatol.*, *5*, 589–606.

Xue, Y., and J. Shukla (1993), The influence of land surface properties on Sahel climate. Part I: Desertification, *J. Clim.*, *6*, 2232–2245.

Xue, Y., P. J. Sellers, J. Kinter, and J. Shukla (1991), A simplified biosphere model for global climates studies, *J. Clim.*, *4*, 354–364.

Zhao, Q., and F.H. Carr (1997), A prognostic cloud scheme for operational NWP models, *Mon. Weather Rev.*, *125*, 1931–1953.

E. J. Burke, Hadley Centre for Climate Prediction and Research, Met Office, FitzRoy Road, Exeter EX1 3PB, UK.

L. G. G. de Goncalves and D. L. Toll, Hydrological Sciences Branch, Code 614.3, NASA Goddard Space Flight Center, Greenbelt, MD 20771, USA. (gustavo@hsb.gsfc.nasa.gov)

S. C. Chou and J. A. Marengo, Centro de Previsão do Tempo e Estudos Climáticos, Instituto Nacional de Pesquisas Espaciais, Cachoeira Paulista, 12630-000 Sao Paulo, Brazil.

P. R. Houser, Center for Research on Environment and Water, George Mason University, 4041 Powder Mill Road, Suite 302, Calverton, MD 20705-3106, USA.

B. Nijssen and W. J. Shuttleworth, Department of Hydrology and Water Resources, University of Arizona, Tucson, AZ 85721, USA.